| | |
|---|---|
| Title | Strengthening mechanisms acting in extruded Mg-based long-period stacking ordered (LPSO)-phase alloys |
| Author(s) | Hagihara, Koji; Li, Zixuan; Yamasaki, Michiaki et al. |
| Citation | Acta Materialia. 2019, 163, p. 226-239 |
| Version Type | VoR |
| URL | https://hdl.handle.net/11094/89825 |
| rights | This article is licensed under a Creative Commons Attribution 4.0 International License. |
| Note | |

Acta Materialia 163 (2019) 226–239

Contents lists available at ScienceDirect

Acta Materialia

journal homepage: www.elsevier.com/locate/actamat

Full length article

# Strengthening mechanisms acting in extruded Mg-based long-period stacking ordered (LPSO)-phase alloys

Koji Hagihara [a, *], Zixuan Li [a], Michiaki Yamasaki [b], Yoshihito Kawamura [b], Takayoshi Nakano [c]

[a] Department of Adaptive Machine Systems, Graduate School of Engineering, Osaka University, 2-1 Yamadaoka, Suita, Osaka, 565-0871, Japan
[b] Magnesium Research Center & Department of Materials Science, Kumamoto University, 2-39-1 Kurokami, Chuo-ku, Kumamoto, 860-8555, Japan
[c] Division of Materials and Manufacturing Science, Graduate School of Engineering, Osaka University, 2-1 Yamadaoka, Suita, Osaka, 565-0871, Japan

ARTICLE INFO

*Article history:*
Received 6 August 2018
Received in revised form
6 October 2018
Accepted 8 October 2018
Available online 10 October 2018

*Keywords:*
Magnesium alloys
Strengthening mechanism
Deformation structure
Extrusion
Deformation kink

ABSTRACT

The unusual increase in the strength by extrusion is a unique feature of recently developed Mg alloys containing the LPSO phase. In this study, we first elucidated the detailed mechanisms that induce this drastic strengthening. The dependencies of the deformation behavior of a $Mg_{88}Zn_4Y_7$ extruded alloy, which contains ~86-vol% LPSO phase, on the temperature, loading orientation, and extrusion ratio were examined. It was found that the yield stress of the alloy is drastically increased by extrusion, but the magnitude of the increase in the yield stress is significantly different depending on the loading orientation. That is, the strengthening of the LPSO phase by extrusion shows a strong anisotropy. By the detailed analyses, this was clarified to be derived from the variation in the deformation mechanisms depending on the loading orientation and extrusion ratio. Basal slip was found to govern the deformation behavior when the loading axis was inclined at a 45° to the extrusion direction, while the predominant deformation mechanism varies from basal slip to the formation of deformation kink bands as the extrusion ratio increased when the loading axis was parallel to the extrusion direction. Moreover, it was clarified in this study that the introduction of a deformation-kink-band boundary during extrusion effectively acts as a strong obstacle to basal slip. That is, "the kink band strengthening" was first quantitatively elucidated, which contributes to the drastic increase in the yield stress of the extruded LPSO-phase alloys in the wide temperature range below 400 °C.

## 1. Introduction

To overcome the problem of global warming, the development of noble lightweight structural materials is strongly desired to improve the fuel efficiency of transportation equipment and vehicles. Mg alloys are strong candidates for achieving this [1], although they generally have some drawbacks such as a low high-temperature strength and low corrosion resistance. As an attempt to improve the mechanical properties of Mg alloys, the usage of the long-period stacking ordered phase, the so-called LPSO phase, has recently received considerable attention [2–15]. The LPSO phase has (0001) close-packed planes in common with the Mg phase with a hexagonal close-packed (hcp) structure. However, the stacking sequence of the (0001) planes along the *c* axis is increased from 2-fold in Mg to 24-, 14-, 18-, or 10-fold in LPSO phases [16]. The plastic deformation mechanism of the LPSO phase was previously examined by using directionally solidified (DS) LPSO-single-phase alloys [17–19]. The dominant deformation mode was identified to be (0001)<11$\bar{2}$0> basal slip in the LPSO phase—the same as that in Mg. In addition, under conditions where the operation of basal slip is difficult, i.e., where the Schmid factor for basal slip is low, the formation of deformation kink bands, which are initiated by the avalanche generation of basal dislocations in a restricted region, also acts as the effective deformation mode [17–21].

The mechanical properties of Mg/LPSO two-phase alloys have been mainly studied for $Mg_{97}Zn_1Y_2$ alloys, in which there is ~24-vol% LPSO phase and the rest is a Mg solid solution. The first finding of the superior mechanical properties of Mg/LPSO two-phase alloys was obtained for a rapidly solidified powder metallurgy alloy [2]. However, Mg/LPSO two-phase alloys with an extremely high strength accompanied by a relatively good ductility have recently

---

* Corresponding author.
*E-mail address:* hagihara@ams.eng.osaka-u.ac.jp (K. Hagihara).

https://doi.org/10.1016/j.actamat.2018.10.016

been realized by conventional thermomechanical processing techniques such as extrusion [4,6–13,15]. In addition, some researchers have studied LPSO-phase alloys, in which the volume fraction of the LPSO phase is drastically increased and regarded as the predominant phase in alloys, to develop alloys with a higher strength [22–27].

The characteristic feature of alloys containing the LPSO phase is that the strength of the alloy in the as-cast state is not very high, but the strength is drastically increased by thermomechanical processing. For example, the yield stress of the $Mg_{97}Zn_1Y_2$ alloy is as low as ~200 MPa [unpublished result], but it increases to ~270 MPa by extrusion at 450 °C with a reduction ratio of 10 [4]. Interestingly, this feature is more obvious in an LPSO-phase alloy. It was previously reported that in a $Mg_{89}Zn_4Y_7$ alloy containing ~86-vol% LPSO phase, the yield stress increases from ~150 MPa in the as-cast state to ~480 MPa in the extruded alloy [22]. That is, the increase in the yield stress by extrusion is ~4.7 times larger in the $Mg_{89}Zn_4Y_7$ alloy than in the $Mg_{97}Zn_1Y_2$ alloy. In the Mg/LPSO two-phase extruded alloy, the short-fiber-like reinforcement by the LPSO phase and the grain refinement effect of the Mg matrix phase by dynamic recrystallization during the extrusion process are found to be the main strengthening mechanisms [4]. However, the strengthening mechanism of the LPSO-phase extruded alloy has not been sufficiently clarified yet. To elucidate this, the variations in the deformation behavior of the extruded LPSO-phase alloy as functions of the extrusion ratio, temperature, and loading orientation were examined in this study. From the results, the unique strengthening mechanisms acting in the extruded LPSO-phase alloy are first clarified, and their contributions are quantitatively estimated.

## 2. Experimental procedure

A master ingot with a composition of $Mg_{89}Zn_4Y_7$ (at%) was prepared by induction melting, followed by casting in a carbon crucible. Then, the as-cast ingots were extruded at 450 °C in air at a constant ram speed of 2.5 mm/s to produce cylindrical specimens. In the extrusion process, specimens with four different reduction ratios of the cross-sectional area of the raw material billet $A_0$ to the cross-sectional area of the extruded bar $A_e$ of 2:1, 3:1, 5:1, and 10:1 were prepared. Hereafter, these extruded alloys are called the R2, R3, R5, and R10 extruded alloys, respectively. These applied reduction ratios were calculated to those that correspond to equivalent strains of 0.7, 1.1, 1.6, and 2.3, respectively [28]. Using these extruded alloys, the influence of the extrusion ratio on the formation of the microstructure and the mechanical properties were examined. The microstructures of the as-cast ingot and the extruded ingots were observed by optical microscopy (OM, Olympus BX60M), scanning electron microscopy (SEM, JEOL JSM-7800F), and transmission electron microscopy (TEM, JEOL JEM-3010). The crystallographic textures in the alloys were examined by electron backscatter diffraction (EBSD) pattern analysis (TSL Instrument, Japan) in the SEM with step sizes of 1 and 0.2 μm for observation of the microstructure and deformation structure, respectively.

Rectangular specimens with dimensions of approximately 2 mm × 2 mm × 5 mm were cut by electrodischarge machining from the as-cast ingot and extruded alloys, and their mechanical properties were measured by compression tests. The tests were conducted in a temperature range between room temperature (RT) and 400 °C in vacuum at a nominal strain rate of $1.67 \times 10^{-4}\ s^{-1}$. Two loading orientations were selected for the compression test to clarify the anisotropic mechanical properties of the extruded alloys; one is parallel to the extrusion direction, and the other is inclined at an angle of 45° from the extrusion direction. The deformation microstructures introduced in the specimens by the compression test were observed by OM with Nomarski interference contrast.

## 3. Results

Fig. 1 shows OM images of the microstructure of the as-cast alloy and its variation in the extruded alloys as a function of the extrusion ratio, observed on the longitudinal section along the extrusion direction. As shown in Fig. 1(a), the LPSO-phase grains showed characteristic thin plate-like shapes, and they were randomly oriented in the as-cast alloy. From TEM observations, the crystal structures of these LPSO phases were confirmed to be the 18R-type LPSO phase, as previously reported [22]. It must be mentioned that the unit cell of the 18R-type LPSO phase shows rhombohedral crystal symmetry. However, in the rhombohedral lattice system, the crystal can also be regarded as possessing a hexagonal structure by considering a unit cell whose volume is three times larger than that of the rhombohedral cell; this allows us to more easily understand the crystal geometry of the LPSO phase. For this reason, the crystal structure of the LPSO-phase is indexed by hexagonal notation in this paper. As a second phase, ~14-vol% Mg-phase grains with round shapes were contained in the alloy, as indicated by the small arrows in Fig. 1(a). The size of the LPSO-phase grains in the cast alloy was relatively small with an average length of ~90 μm and a thickness of ~10 μm. By extrusion, the crystal structure of the LPSO phase was unchanged irrespective of the extrusion ratio. In addition, dynamic recrystallization did not occur macroscopically in the LPSO phase grains, even in the extrusion at 450 °C. This was previously confirmed by TEM observations of R10 extruded alloys, although the formation of tiny recrystallized grains was reported in the local vicinity of the grain boundary [22]. On the other hand, the morphologies of the grains were largely varied due to the extrusion. The plate-like shapes of the LPSO-phase grains were rotated by extrusion and tended to align along the extrusion direction. The directionality of the alignment along the extrusion direction became stronger as the extrusion ratio increased, as observed in Fig. 1(b)–(e).

Such a variation in microstructure can be more clearly confirmed by the crystallographic texture analysis using SEM. Fig. 2 shows the crystal orientation maps of the LPSO phase, and Fig. 3 shows the corresponding (0001), $\{10\bar{1}0\}$, and $\{11\bar{2}0\}$ pole figures showing the variation in the texture with the extrusion ratio, analyzed on the transverse section of the extruded alloy by SEM-EBSD analysis. As shown in Fig. 3(a), the intensities of the (0001) poles were randomly distributed in the as-cast alloy, but the intensities of the (0001) poles in the extruded alloys tended to be located at the outer circumference in the pole figure; that is, the (0001) planes were aligned parallel to the extrusion direction. In previous studies, it was reported that the wide interface of the plate-like shape of an LPSO-phase grain is parallel to (0001) [17]. Thus, the formation of the aligned microstructure in Fig. 1 by extrusion is in good agreement with the development of the ring-like shape of the (0001) pole figure along the extrusion direction in Fig. 3. The intensity profile of (0001) in the pole figure became sharper as the extrusion ratio increased. In addition, as the extrusion ratio increased, the intensity concentration of the $\{10\bar{1}0\}$ poles at the center, i.e., along the extrusion direction, became significant. This feature is similar to that observed in conventional extruded Mg alloys [29]. Mayama et al. studied the mechanisms for the development of the texture of hcp Mg in the extrusion process using a computational simulation based on a finite-element crystal plasticity analysis [30]. They argued that in addition to basal slip, a nonbasal slip system with the same $<1\bar{2}10>$ Burgers vector plays an important role in the development of such a $\{10\bar{1}0\}$ fiber texture along the extrusion direction. A similar mechanism may be

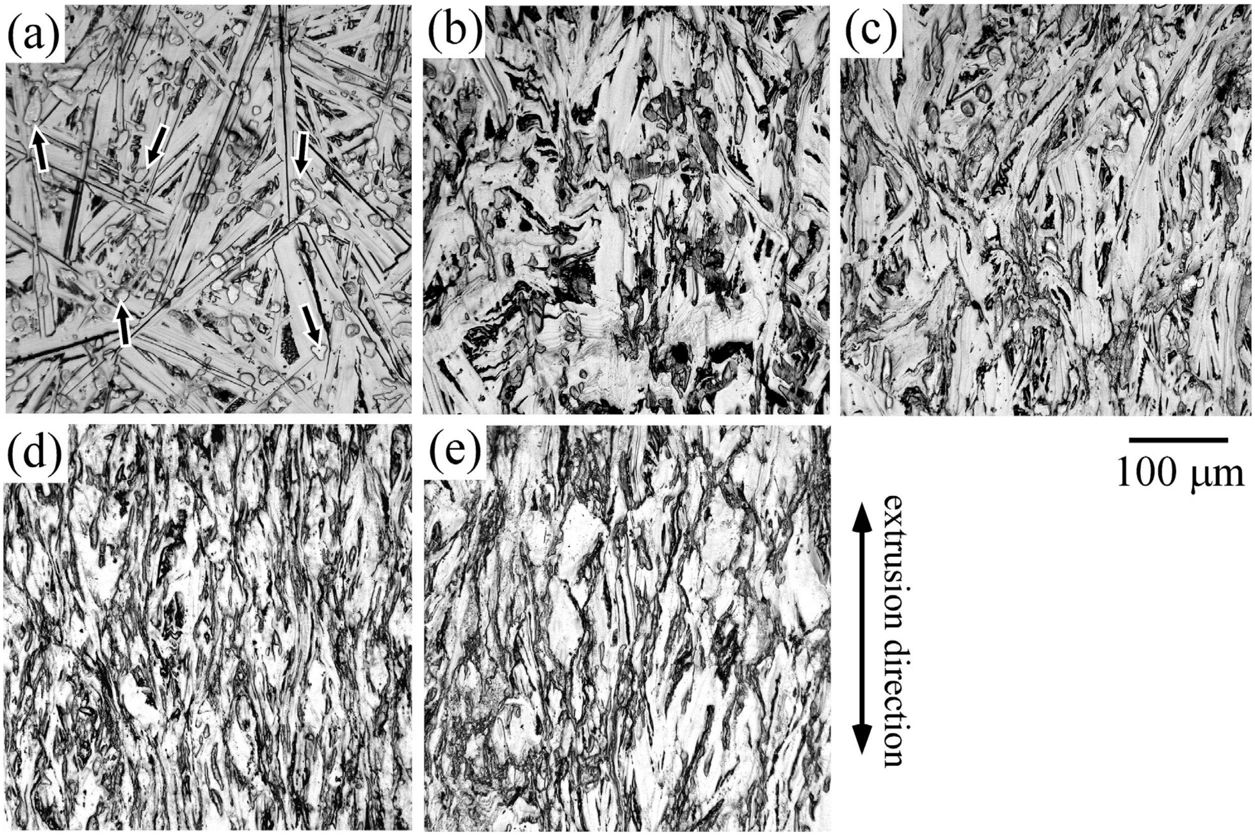

**Fig. 1.** OM images of the microstructure of the as-cast alloy and its variation in the extruded alloys as a function of the extrusion ratio observed on the longitudinal section along the extrusion direction: (a) as-cast alloy and extruded alloys (b) R2, (c) R3, (d) R5, and (e) R10.

applicable to this LPSO-phase alloy since the operation of $\{10\overline{1}0\}$ prismatic slip in the LPSO phase has also been reported, especially at high temperatures at and above 400 °C [31]. In Fig. 2, the “apparent” grain size of the LPSO phase seems to decrease as the extrusion ratio increases. However, this does not actually occur and was caused by the increase in the stored strain in the LPSO-phase grains, which hinders the detection of the clear EBSD pattern for crystal orientation analysis.

Fig. 4 shows higher-magnification images of the microstructures of the extruded alloys observed on the longitudinal section. No occurrence of the macroscopic recrystallization of LPSO phase grains is confirmed in the images. Instead, it is noted that there is significant bending and rounding of the (0001) interface of the LPSO-phase grains in the extruded alloy accompanied by the alignment of the plate-like grains along the extrusion direction. This was caused by the introduction of many deformation bands, as expected their boundaries are indicated by the red dashed lines in the images. The bending of the LPSO-phase grains was significant even in the R2 extruded alloy, and the frequency and magnitude of the bending seemed to gradually increase as the extrusion ratio increased. Fig. 5(a) and (b) show the typical crystal orientation maps of the bent region of an LPSO-phase grain in the R2 extruded alloy. In addition, the (0001), $\{10\overline{1}0\}$, and $\{11\overline{2}0\}$ pole figures taken in Region A–D are presented in Fig. 5(c). The (0001) pole figures indicate that large crystal rotation occurred in the bent regions. Between Points A and B in Fig. 5(a), crystal rotation occurred along the $<5\ \overline{23}\ 18\ 0>$ axis, which is close to $<0\overline{1}10>$ with a large rotation angle of 22.4°. It is noted that the crystallographic features of the bent region were examined at some other positions, and it is clarified that the rotation angle is not unique, as shown in Fig. 5(b). At Points C and D, crystal rotation occurred along the $<8\ \overline{21}\ 13\ 0>$ axis, which is close to $<1\overline{2}10>$, with a rotation angle of 12.4°. This demonstrates that both the rotation angle and rotation axis in the deformation band were different in each band, although the rotation axis is almost perpendicular to [0001] in most of the bent region. Such arbitrariness of the rotation angle and rotation axis in the deformation bands is in good agreement with that measured for a deformed LPSO phase [20,21,32] and is different from that observed for conventional deformation twins. This demonstrates that the bending of the LPSO-phase grain occurs by the formation of deformation kink bands during the extrusion process, which are initiated by the avalanche generation of basal dislocation in a restricted region.

Focusing on these as-cast and extruded alloys, compression tests were conducted to examine the mechanical properties. Fig. 6(a) and (b) show the temperature dependence of the yield stress in the 0° and 45° loading orientation, i.e., deformed parallel to the extrusion direction and inclined at an angle of 45° with respect to this direction, respectively. The yield stress of the as-cast alloy was as low as ~140 MPa at RT. However, the yield stress drastically increased by extrusion, as briefly described in Section 1. Note that the magnitude of the increase in the yield stress was found to show significant variations with the loading orientation and extrusion ratio. For deformation in the 0° loading orientation at RT, the yield stress increased by almost two times compared to that of the as-cast alloy by the extrusion of R2. The magnitude of the increase in the yield stress monotonically increased as the extrusion ratio increased. Further, the yield stress of the R10 extruded alloy reached ~460 MPa, i.e., ~3.3 times higher than that of the as-cast alloy. Even at 200 °C, the yield stress was nearly comparable for

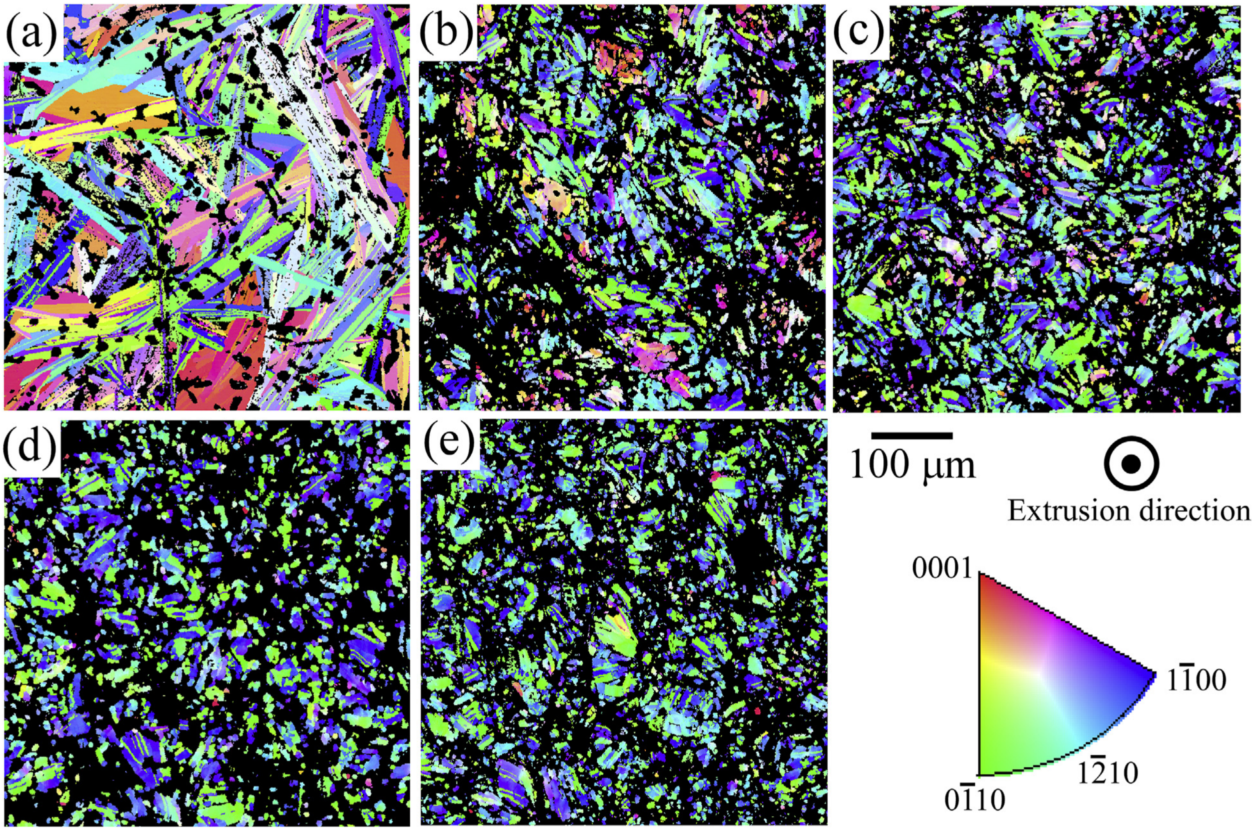

**Fig. 2.** Crystal orientation maps showing the variations in the texture developed in the $Mg_{89}Zn_4Y_7$ alloys by extrusion at different extrusion ratios, acquired by an SEM-EBSD analysis of the transverse section along the extrusion direction: (a) as-cast alloy and extruded alloys (b) R2, (c) R3, (d) R5, and (e) R10.

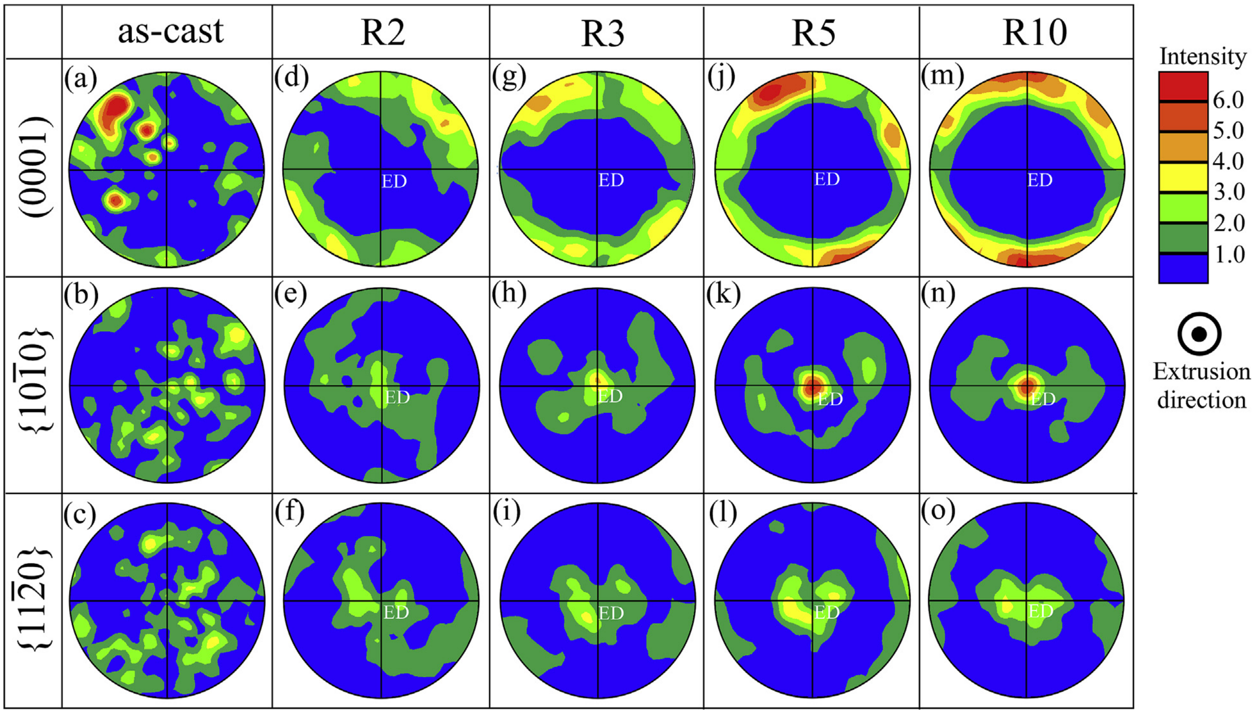

**Fig. 3.** Variations in the pole figures of the as-cast and extruded $Mg_{89}Zn_4Y_7$ alloys, as analyzed by crystal orientation maps taken on the transverse section along the extrusion direction in Fig. 2(a)–(e): (a), (d), (g), (j), and (m) {0001}; (b), (e), (h), (k), and (n) {10$\bar{1}$0}; and (c), (f), (i), (l), and (o) {11$\bar{2}$0} pole figures.

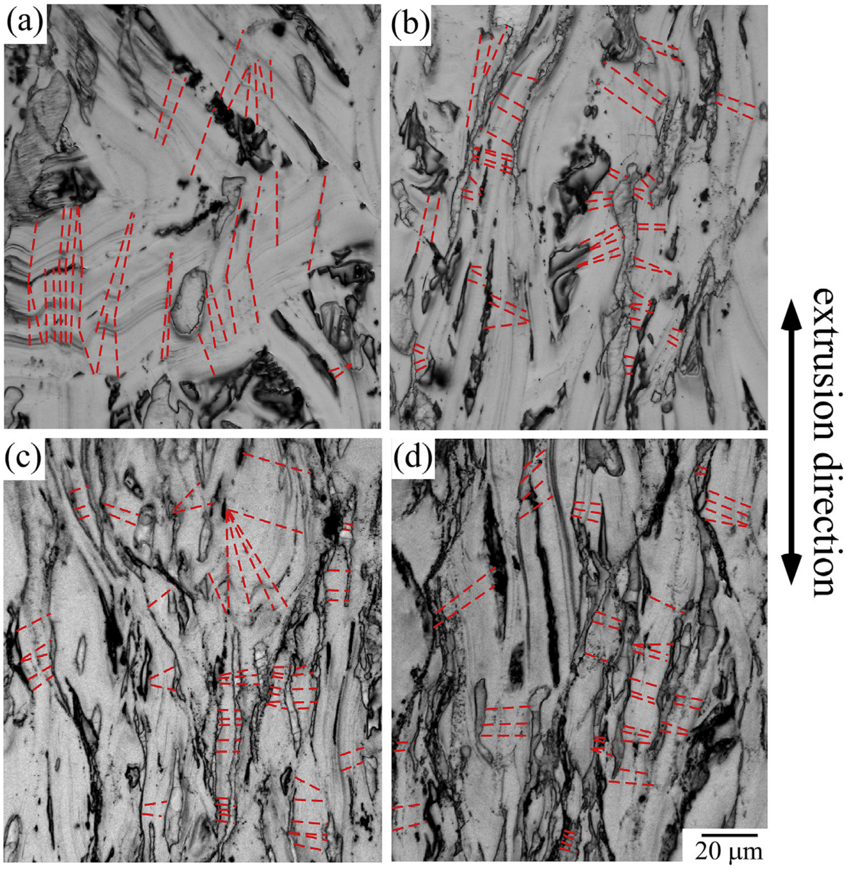

**Fig. 4.** Higher-magnification images of the microstructures of the extruded alloys with different extrusion ratios: (a) R2, (b) R3, (c) R5, and (d) R10 observed on the longitudinal section along the extrusion direction. The positions at which deformation-kink-band boundaries are expected to exist from the microstructures are indicated by the red dashed lines. (For interpretation of the references to color in this figure legend, the reader is referred to the Web version of this article.)

all specimens at RT; that is, the strengthening of the alloy was maintained in all the extruded alloys. At 300 °C, however, the yield stress showed a notable decrease. Note that the magnitude of the decrease in the yield stress was different for each specimen; it was larger for a specimen with a higher extrusion ratio. Thus, the yield stress of the R10 extruded alloy showed a drastic decrease compared to the others. The yield stress showed a large scatter compared to the values reported in a previous study [33] at 300 °C, probably owing to the slight fluctuation in the alloy composition and its strong variation with temperature. Because of the drastic decrease in the yield stress of the R10 extruded alloy, it showed almost the same yield stress as that of the R5 extruded alloy at 300 °C. The drastic decrease in the yield stress continued up to 400 °C for extruded alloys with high extrusion ratios. As a result, the yield stresses of the extruded alloys showed lower values as the extrusion ratio increased at and above 350 °C, which is the opposite trend observed at low temperatures.

An increase in the yield stress due to an increase in the extrusion ratio was also observed for the yield stresses obtained in the 45° loading orientation, but the detailed features were much different from those observed in the 0° loading orientation, as shown in Fig. 6(b). The magnitude of the increase in the yield stress for the extruded alloys compared to that for the as-cast alloy became larger as the extrusion ratio increased, but the absolute value of the difference in the yield stress depending on the extrusion ratio was much smaller than that measured in the 0° loading orientation. That is, at RT, the yield stress largely increased from ~140 MPa up to ~220 MPa by the extrusion of R2, but the increase in the yield stress with the increase in the extrusion ratio was much smaller than that in the 0° loading orientation. The difference in the yield stresses for the R2 and R10 extruded alloys was as small as ~50 MPa, compared to ~200 MPa in the 0° loading orientation. The yield stresses at 200 °C were almost comparable to those at RT. At 300 °C, the yield stress of the extruded alloy slightly decreased. The magnitude of the decrease was larger for alloys with a larger extrusion ratio, but all of the extruded alloys maintained much higher yield stresses than that of the as-cast alloy. However, the yield stress of the extruded alloy drastically decreased at higher temperatures around 400 °C, and the yield stress of the extruded alloy was lower than that of the as-cast alloy. Note that the yield stresses of the extruded alloys at 400 °C showed lower values as the extrusion ratio increased, similar to that observed in the 0° loading orientation.

To discuss the anisotropy of the yield stress quantitatively, Fig. 6(c) shows the yield stress ratio $\sigma_0/\sigma_{45}$ as a function of the temperature. In all alloys, the yield stress was higher in the 0° orientation than that in the 45° orientation for all temperatures investigated. The anisotropy of the yield stress was larger for alloys with a higher extrusion ratio, and it was especially significant at low temperatures below 200 °C for the R3, R5, and R10 extruded alloys. At and above 300 °C, however, the difference in the anisotropy with the extrusion ratio became drastically small and was diminished at 400 °C.

Fig. 7(a) and (b) show the stress–strain curves obtained from the compression tests in the 0° and 45° loading orientations, respectively. It is noted that in addition to the difference in the yield stress, the work-hardening rates in the stress–strain curves are

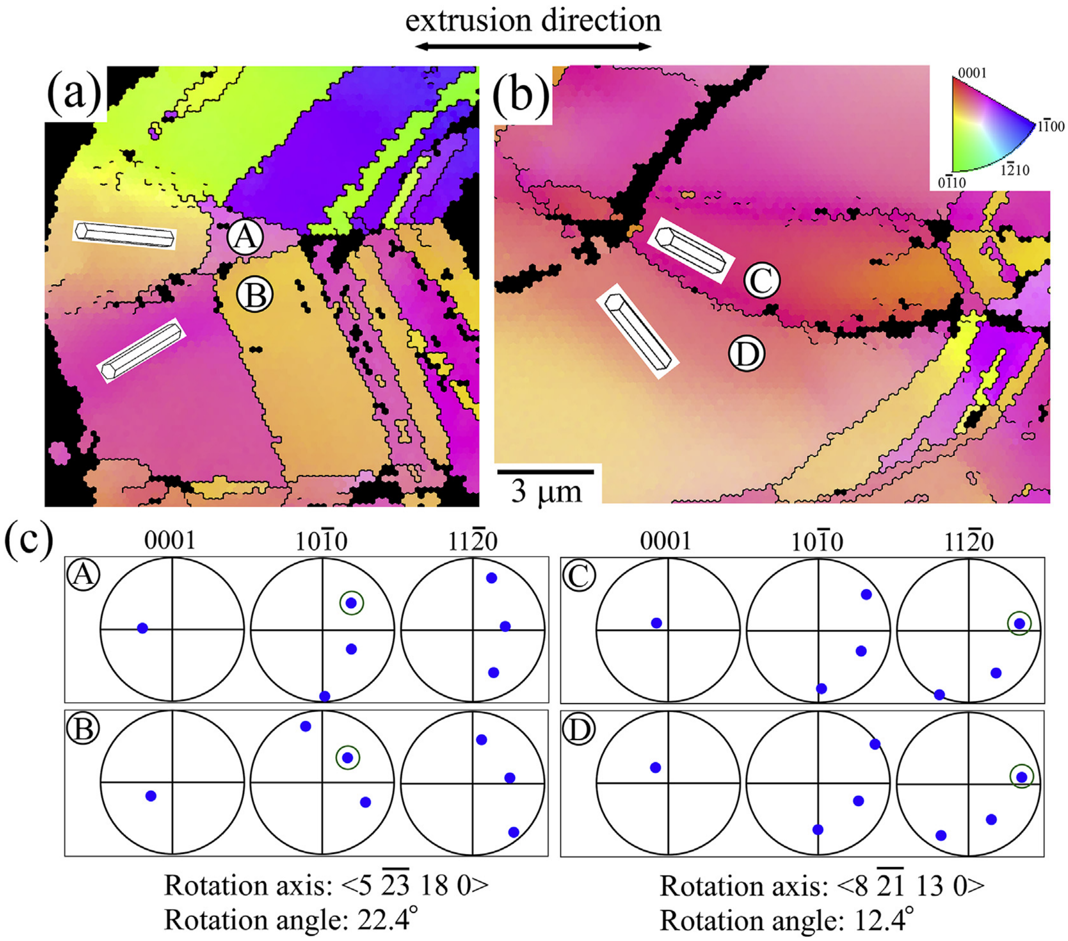

**Fig. 5.** (a), (b) Typical examples of crystal orientation maps of the bent region of an LPSO phase grain for extruded specimen R2. (c) (0001), $\{10\bar{1}0\}$, and $\{11\bar{2}0\}$ pole figures taken at Points A–D in Fig. 5(a) and (b).

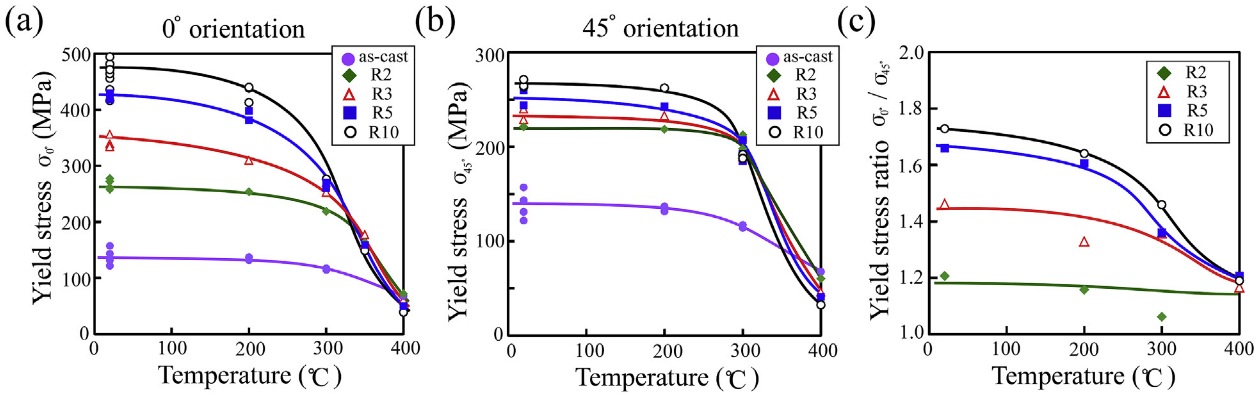

**Fig. 6.** Temperature dependence of the yield stress of the $Mg_{89}Zn_4Y_7$ as-cast and extruded alloys measured by compression tests in the (a) 0° ($\sigma_0$) and (b) 45° orientations ($\sigma_{45}$). (c) Variation in the yield stress ratio $\sigma_0/\sigma_{45}$ as a function of the temperature for the extruded alloys.

largely different for the 0° and 45° loading orientations. To discuss this quantitatively, the variations in the differential value of $\Delta\sigma/\Delta\varepsilon$ with the plastic strain, where $\sigma$ is the flow stress and $\varepsilon$ is the plastic strain, were evaluated from the stress-strain curves, and the work-hardening behaviors of each alloy were compared. As a typical example of differences in work-hardening behaviors, Fig. 7(c) and (d) show the work-hardening rate, $\Delta\sigma/\Delta\varepsilon$, measured at 2% plastic strain in the 0° and 45° loading orientations, respectively, as a function of the extrusion ratio and testing temperature. The work-hardening rate of the as-cast alloy exhibits a relatively high value of ~30 MPa/1% at RT, and nearly comparable work-hardening rates were measured for all of the extruded alloys for deformation in the 45° orientation at RT, independent of the extrusion rate. For deformation in the 0° orientation, a slightly small but nearly comparable work-hardening rate compared to that in the 45° orientation was measured for the R2 extruded alloy. However, this

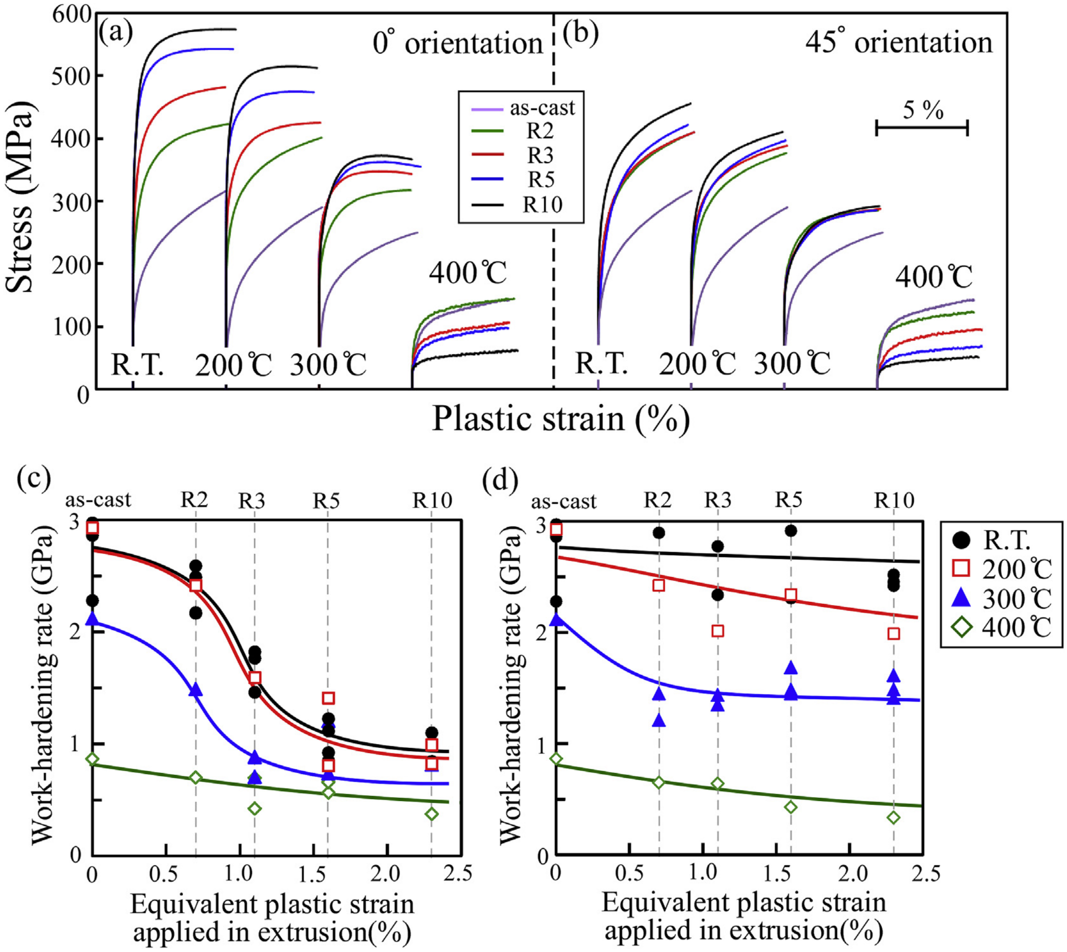

**Fig. 7.** (a), (b) Typical stress–strain curves measured from compression tests of the $Mg_{89}Zn_4Y_7$ alloys. (c), (d) Variation in work-hardening rate measured at 2% plastic strain as a function of the temperature and extrusion ratio in the (a), (c) 0° and (b), (d) 45° orientations.

value drastically decreased as the extrusion ratio increased. Further, the work-hardening rate showed a low value of ~10 MPa/1% for the R5 and R10 extruded alloys. A similar work-hardening rate was maintained at 200 °C for both loading orientations. At 300 °C, however, the work-hardening rate largely decreased, especially for the extruded alloys deformed in the 45° orientation. At 400 °C, the work-hardening rate of the as-cast alloy drastically decreased to a value as small as ~9 MPa/1%, and further smaller work-hardening rates were measured for extruded alloys in both loading orientations. These results strongly suggest that the mechanisms controlling the deformation behavior of the extruded specimens vary with the extrusion ratio, loading orientation, and temperature. This idea is supported by observations of the deformation microstructures as follows.

Fig. 8 shows OM images of the typical deformation microstructures introduced in the alloys by compression tests to ~5% plastic strain at various temperatures. Fig. 8(a)–(c) show the deformation microstructure of the as-cast alloys and those of the extruded alloys deformed in the 0° and 45° orientations, respectively. In the as-cast alloy, the localized introduction of slip traces was observed as indicated by red arrows. The slip traces were concentrated in some specific grains and were introduced parallel to the long interface of the grains. The features of the deformation microstructures were almost the same at all of the temperatures investigated. These observations demonstrate that (0001) basal slip is the predominant deformation mechanism at all testing temperatures for the as-cast specimen since the plate-like interface of an LPSO-phase grain is parallel to (0001). The Burgers vector for (0001) slip was previously determined to be parallel to <11$\bar{2}$0> in an 18R-LPSO-phase crystal [17]. Similar features of the deformation microstructures were observed for a specimen deformed in the 45° loading orientation, as shown in Fig. 8(b). No difference in the deformation microstructure depending on the extrusion ratio and testing temperature was confirmed in the 45° orientation, except for deformation at 400 °C. At 400 °C, the number of basal slip traces was reduced, and strong wavy contrast along the grain boundary was instead frequently observed.

On the other hand, a different deformation microstructure was observed for the extruded alloys deformed in the 0° orientation depending on the extrusion ratio. In the R2 extruded alloy, a deformation microstructure similar to those in the 45° orientation, i.e., the introduction of basal slip traces, was observed in the temperature range between RT and 300 °C. The number of basal slip traces was reduced in the R3 extruded specimens, and deformation bands with unique lenticular shapes were introduced instead, as indicated by blue arrows. The number of deformation bands with lenticular shapes was further increased for the R5 and R10 extruded alloys. Most of the lenticular deformation bands were introduced almost perpendicular to the long interface of the LPSO-phase grains.

Fig. 9 shows a typical example of the crystal orientation map of the deformation bands with lenticular shapes introduced by

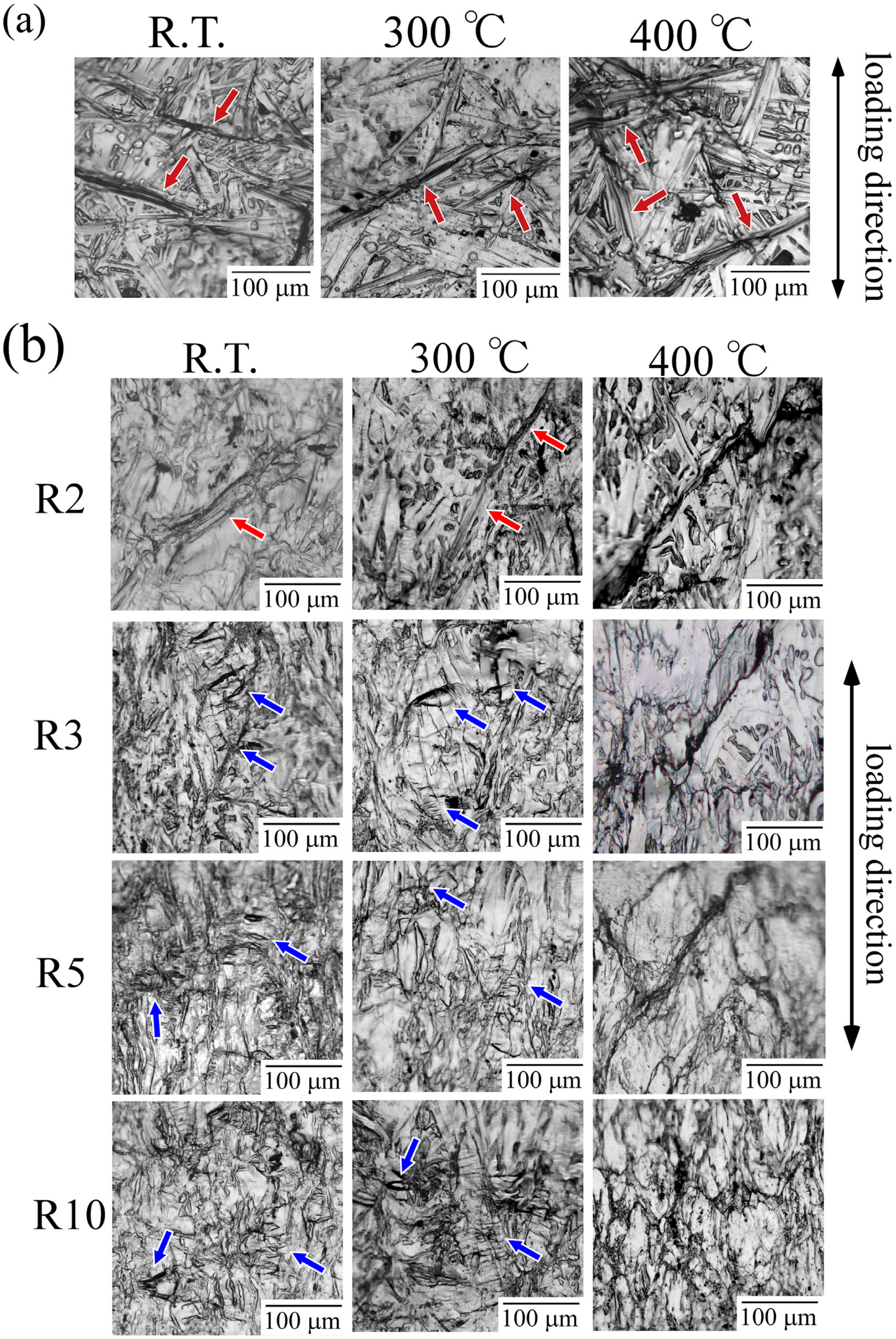

**Fig. 8.** OM images showing the typical deformation microstructures introduced in the specimens by the compression tests to ~5% plastic strain as a function of the loading orientation, temperature, and extrusion ratio: (a) as-cast alloys and extruded alloys deformed in the (b) 0° and (c) 45° orientations. The red and blue arrows indicate the traces of basal slip and deformation band, respectively. (For interpretation of the references to color in this figure legend, the reader is referred to the Web version of this article.)

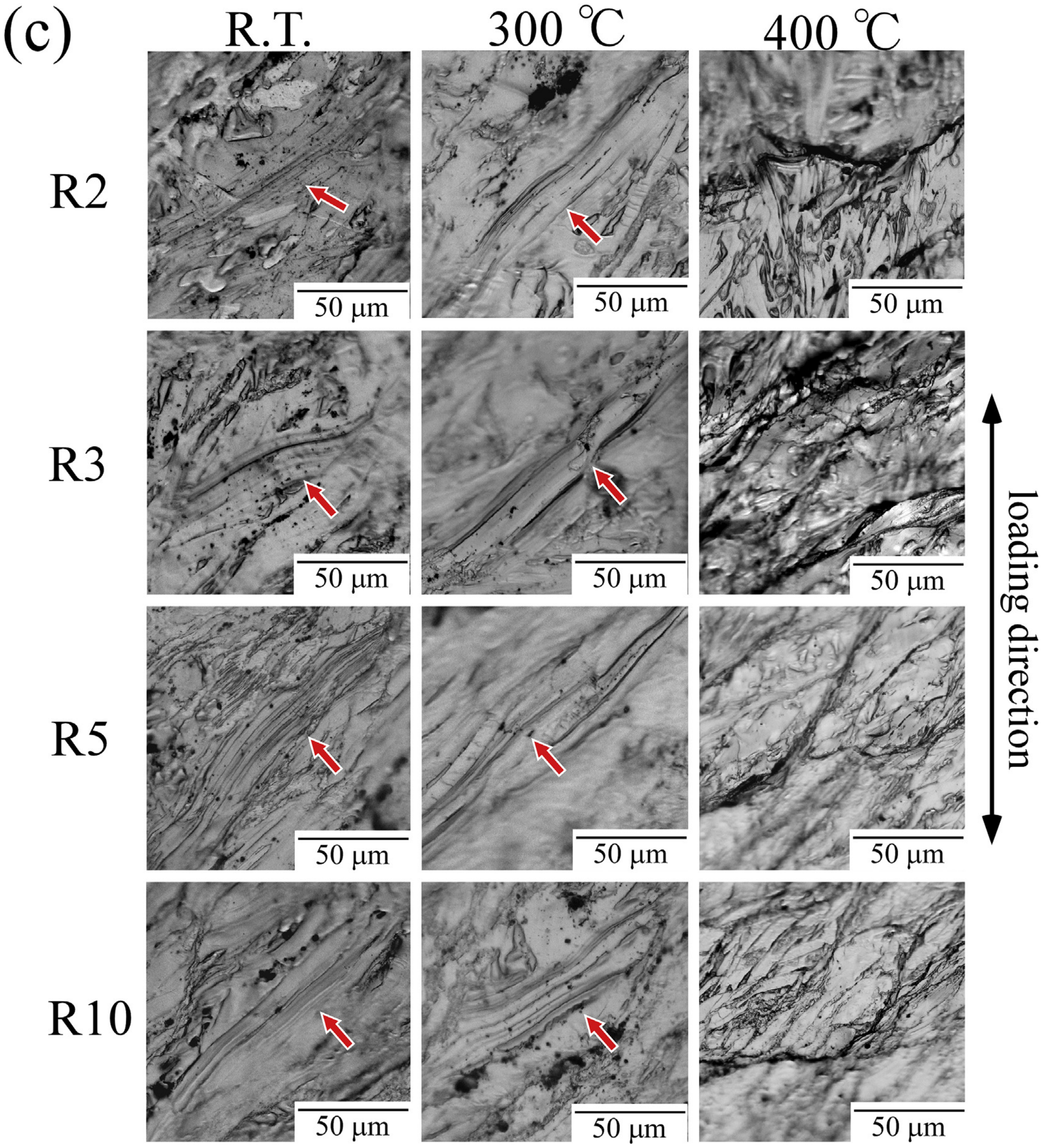

**Fig. 8.** (*continued*).

deformation in the 0° orientation. Similar crystallographic features to those monitored in the as-extruded alloys shown in Fig. 4 were observed. That is, the deformation bands had an arbitrary crystal rotation axis perpendicular to the *c* axis, and the crystal rotation angle was different for each band. This indicates that the introduced deformation bands are also the deformation kink bands formed by compressive deformation.

For deformation at 400 °C, the number of deformation kink bands decreased. Instead, localized shear deformation along the grain interface was frequently observed, which is similar to that observed in the 45° orientation at 400 °C.

Note that the present results on the variations in the operative deformation mode in the extruded LPSO-phase alloy depending on the loading orientation are in good agreement with results recently reported by Garces et al. [27]. They examined the orientation dependence of the mechanical properties of a $Mg_{88}Zn_5Y_7$ (at%) extruded alloy in which the volume faction of the LPSO phase was ~95%, and reported that the yield stress along the extrusion direction (0° orientation in this study) was much higher than the yield stress along the direction 45°-tilted from the extrusion direction toward the transverse direction (45° orientation in this study) [25,27]. To clarify the origin of this behavior, they conducted the study combined with the in-situ X-ray synchrotron diffraction experiments and acoustic emission testing. As a result, basal slip and formation of deformation kink bands were identified to be the predominant deformation mechanisms in the early stage of the plastic deformation of the extruded $Mg_{88}Zn_5Y_7$ alloy at 45° and 0° loading orientations, respectively, under compression at RT [27]. This is the same conclusion obtained in the present study.

## 4. Discussion

It was clarified that the yield stress of the $Mg_{89}Zn_4Y_7$ LPSO-phase alloy was drastically increased by extrusion. It should be emphasized that the yield stress increased as the extrusion ratio increased, but the magnitude of the increase in the yield stress is significantly different depending on the loading orientation. That is, the strengthening of the LPSO phase by extrusion shows a strong anisotropy. The variation in the mechanisms controlling plastic deformation depending on the loading orientation and extrusion

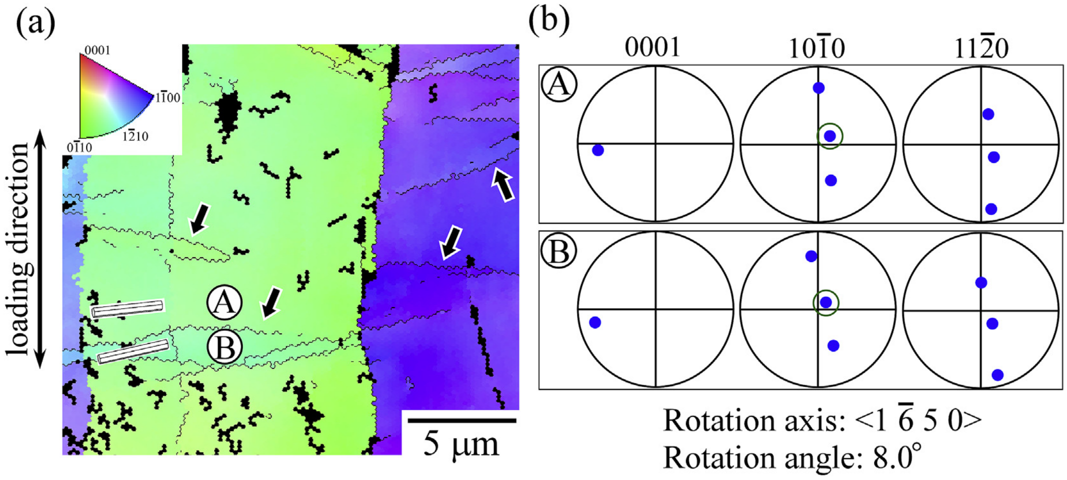

**Fig. 9.** (a) Typical example of a crystal orientation map of the deformation bands with lenticular shapes introduced by deformation of the extruded specimen R5 in the 0° orientation at RT. The introduced deformation bands were indicated by arrows. (b) (0001), {10$\bar{1}$0}, and {11$\bar{2}$0} pole figures taken at Points A and B in Fig. 9(a).

ratio was suggested as its origin. In this section, the strengthening mechanisms acting in the extruded LPSO-phase alloy are discussed in detail.

### 4.1. Strengthening mechanisms acting in the 45° orientation

From the observations of the deformation microstructures shown in Fig. 8, (0001)<11$\bar{2}$0> basal slip and the formation of deformation kink bands were suggested as the predominant deformation mechanisms of the extruded LPSO-phase alloys. We first focus on the deformation behavior by basal slip. It is well-known that the activity of (0001) basal slip in Mg alloys is strongly dependent on the texture [34] due to the low crystal symmetry of the hcp structure compared to {111} slip in face-centered cubic (fcc) crystals. This is applicable to the LPSO phase. By using the results of the SEM-EBSD analysis in Fig. 2, the average value of the Schmid factor for basal slip in LPSO-phase grains, $SF_{ave}$, was estimated in cast and extruded alloys. Using the data acquisition software TSL-OIM Analysis Ver.7, a color map showing the maximum Schmid factor value for the (0001)<11$\bar{2}$0> slip at each measured pixel was created with the incremental steps (bin width) of the Schmid factor of 0.05, and the distribution of area fractions of pixels having Schmid factor values in the specified ranges, $A_f$, were evaluated as a histogram. That is, the area fraction of the pixels in the SEM-EBSD images showing Schmid factors between 0 and 0.05 is X%, 0.05–0.10 is Y%, ····, and 0.45–0.50 is Z%. Using these values, the average Schmid factor in the LPSO-phase grains $SF_{ave}$ was evaluated as the summation of the products of the intermediate value of Schmid factor in the evaluated range, $SF_{int}$, and the measured area fraction $A_f$, as follows;

$$SF_{ave} = \sum_i SF_{int,\,i} \cdot A_{f,\,i} \tag{1}$$

In the above example, the $SF_{ave}$ is estimated to be 0.025 × X/100 + 0.075 × Y/100 + …. + 0.475 × Z/100. The evaluated average Schmid factor values for the 0° and 45° loading orientations are shown in Fig. 10. The average Schmid factor was estimated to be ~0.33 for the as-cast alloy. It is to be noted that the average Schmid factor for the extruded alloys in the 45° loading orientation is almost unchanged and independent of the extrusion ratio, and the value is almost comparable to that of the as-cast alloy. On the other hand, the average Schmid factor for basal slip drastically decreased as the extrusion ratio increased for the 0° orientation owing to the development of a {10$\bar{1}$0} fiber texture in which the basal planes tend to align parallel to the extrusion direction, i.e., along the 0° loading orientation, as clarified in Fig. 3. The development of this {10$\bar{1}$0} fiber texture must be one of the origins of the drastic increase in the yield stress by extrusion via the suppression of the easy operation of basal slip. The significant increase in the yield stress in the 0° orientation compared to that in the 45° orientation at low temperatures can be explained by the differences in the variation in the average Schmid factor depending on the loading axis in Fig. 10.

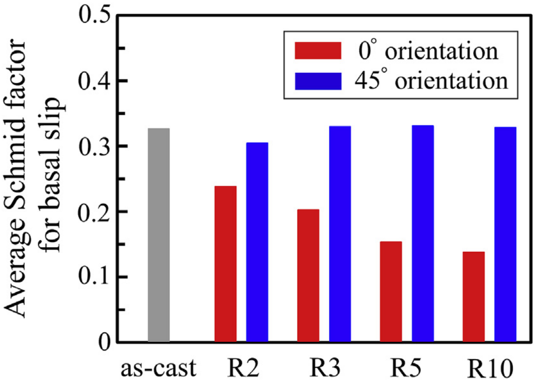

**Fig. 10.** Average Schmid factor for basal slip in the LPSO-phase grains in the extruded alloys deformed in the 0° and 45° loading orientations, evaluated by the crystal orientation maps shown in Fig. 2.

In addition to this texture effect, the results of the present study suggest that the introduction of deformation kink bands during the extrusion process also significantly contributed to the increase in the yield stress. This can be clarified by the following analysis. Here, assuming that the yielding of all specimens during deformation occurs only by the operation of basal slip, the apparent critical resolved shear stress (CRSS) for basal slip can be evaluated by the product of the average Schmid factor in Fig. 10 and the experimentally obtained yield stress in Fig. 5. The calculation results are plotted in Fig. 11 for both the 0° and 45° orientations. For the 45° orientation, the apparent CRSS of the as-cast alloy is ~45 MPa at RT, but it largely increased to ~65 MPa by the extrusion at the ratio of R2. Although the rate of increase became moderate, the apparent CRSS tended to show a monotonic increase as the extrusion ratio

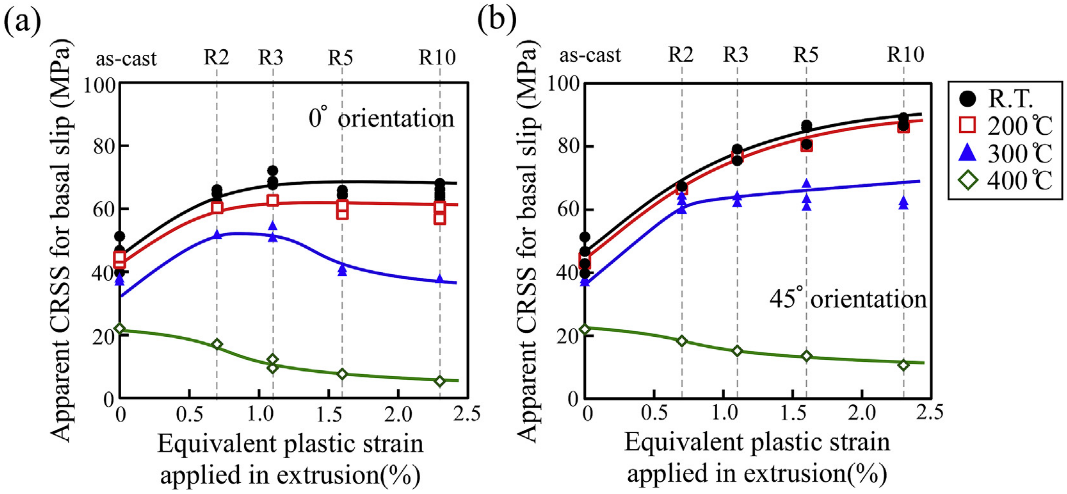

**Fig. 11.** Variation in the apparent CRSS for basal slip with the extrusion ratio and temperature in the (a) 0° and (b) 45° orientations.

increased at RT. An almost similar tendency was observed at 200 °C. Although the rate of increase became moderate, the increase in the apparent CRSS relative to that of the as-cast alloy was maintained even at 300 °C. This strong increase in the apparent CRSS for basal slip at temperatures lower than 300 °C must be brought about by the introduction of deformation kink bands during the extrusion process. Since a kink band boundary is introduced perpendicular to the basal slip plane [15–19], it must act as a strong obstacle against the motion of basal dislocations. In addition to the effects of the deformation kink bands, the effects of the introduction of dislocations during the extrusion process, which induce work-hardening, are also supposed. We confirmed, however, that even after annealing the specimen at 300 °C for 1 week to reduce the dislocation density, there are almost no changes in stress–strain curve for the specimen deformed in the 45° orientation. The cyclic annealing treatment between 200 and 250 °C was also conducted, but the result was the same. This implies that the effects of the introduction of dislocations are small for strengthening in the 45° orientation; instead, the effects of the kink bands must be predominant. To elucidate the physical origin of the "deformation-kink-band strengthening" more clearly, a model study using a directionally solidified LPSO-phase single-phase crystal is now ongoing by our group. The results will be described elsewhere.

At 400 °C, on the other hand, the "apparent" CRSS decreased as the extrusion ratio increased. It is unlikely that this decrease was brought about by an actual decrease in the CRSS for basal slip by an increase in the extrusion ratio. Instead, the result suggests that the mechanism controlling the deformation varied from basal slip to another unknown deformation mechanism at 400 °C.

### 4.2. *Strengthening mechanisms acting in the 0° orientation*

For deformation in the 0° orientation, the relation between the apparent CRSS for basal slip and the extrusion ratio was largely different from that in the 45° orientation, as shown in Fig. 11(a). At RT, the apparent CRSS showed a drastic increase for the R2 extruded alloy compared to that for the as-cast alloy. The magnitude of the increase in the CRSS is almost the same as that observed in the 45° orientation. Similar increases in the apparent CRSS comparable to those in the 45° orientation were measured also at 200 and 300 °C for the R2 extruded alloy. This demonstrates that basal slip is the mechanism controlling the deformation for the R2 extruded alloy even in the 0° orientation. This is because the development of a $\{10\bar{1}0\}$ fiber texture is not too significant to suppress the occurrence of basal slip. However, a further increase in the extrusion ratio did not induce an increase in the apparent CRSS for basal slip. That is, the apparent CRSS showed almost constant values for the R3, R5, and R10 extruded alloys at RT and 200 °C, which is different from the behavior for the 45° orientation. Furthermore, the apparent CRSS slightly decreased as the extrusion ratio increased for the R3, R5, and R10 extruded alloys at 300 °C. This indicates that the mechanism controlling the deformation in the 0° orientation varied with the extrusion ratio for R2 and R3. The deformation microstructures in Fig. 8 suggest that basal slip and the formation of lenticular-shaped deformation kink bands control the plastic deformation in alloys with lower and higher extrusion ratios, respectively. Note that this assumption is in good agreement with the variation in the work-hardening rate from the stress–strain curves in Fig. 7. That is, the greater work-hardening was observed for the R2 extruded alloy, in which basal slip controls the deformation behavior, while the work-hardening rate decreased for the alloys with an extrusion ratio larger than R3, in which the formation of deformation kink bands governs the deformation behavior. This idea is in good agreement with the high work-hardening rate measured in the 45° orientation in Fig. 7(b) and (d), in which basal slip controls the deformation behavior. As one of the origins of the stronger work-hardening rate measured for basal slip, the influence of the deformation kink bands introduced during the extrusion process is strongly considered. The deformation-kink-band boundaries were introduced nearly perpendicular to the basal slip plane. Thus, they must act as strong obstacles for the motion of basal dislocations, inducing a large work-hardening rate. On the other hand, the pre-existing deformation kink bands may barely affect the formation behavior of new deformation kink bands during the compression test. This is because a deformation kink band is known to form perpendicular to a plate-like grain boundary in any situation, as shown in Fig. 9. Thus, deformation kinks are formed parallel to a pre-existing kink band boundary without intersecting each other during the compression test. As a result, a lower work-hardening rate would be measured for extruded alloys with high extrusion ratios in the 0° orientation. Rather, there is a possibility that the pre-introduced kink band boundary might act as the initiation site for the formation of new kink band boundaries, as was suggested by the in-situ observations of the deformation behavior in a directionally solidified LPSO-phase crystal [35]. However, further studies are required to examine this.

On the basis of the abovementioned considerations, the effects of the strengthening mechanisms contributing to the increase in the yield stress of the extruded alloy deformed in the 0° orientation were quantitatively estimated, as shown in Fig. 12(a)–(d), as a function of the extrusion ratio and testing temperature. Fig. 12(a) shows the variation in the yield stress with the extrusion ratio at RT. First, the texture effect, i.e., the reduction in the average Schmid factor for basal slip by the development of a $\{10\bar{1}0\}$ fiber texture, is considered. This effect can be quantitatively estimated by dividing the CRSS for basal slip evaluated for the as-cast alloy by the average Schmid factor for basal slip shown in Fig. 10. This texture effect is indicated by the blue bars in Fig. 12(a). In addition, deformation-kink-band strengthening, i.e., the increase in the apparent CRSS for basal slip by the introduction of deformation-kink-band boundaries, is considered as another strengthening effect induced by extrusion, as described above. The magnitude of the increase in the CRSS for basal slip as a function of the extrusion ratio could be quantitatively evaluated by the test in the 45° orientation, as shown in Fig. 11(b). Thus, this additional effect by “deformation-kink-band strengthening” in the 0° orientation can be quantitatively evaluated by dividing the apparent CRSS evaluated for the extruded alloys deformed in the 45° orientation (Fig. 11(b)) by the average Schmid factor for basal slip in the 0° orientation, as indicated by the red bars. Note that the experimentally measured yield stress in the R2 extruded alloy at RT is almost in good agreement with the red bar, indicating that almost only basal slip governs the yield stress of the R2 extruded alloy, as expected. On the other hand, for the R3, R5, and R10 extruded alloys, the expected yield stress by “deformation-kink-band strengthening” is larger than the actually measured yield stress. It is obvious that the reduction in the yield stress compared to the expected yield stress by kink-band strengthening is brought about by the formation of “new” deformation kink bands during the compression test, as observed in Fig. 8(b). This result demonstrates that the deformation kink bands in the LPSO phase play multiple roles—not only as a strengthening component against basal slip to increase the yield stress, but as a “deformation mode” to induce the deformability of the LPSO phase.

Such texture and deformation-kink-band strengthening effects effectively increase the yield stress up to 200 °C, as shown in Fig. 12(b). At 300 °C, however, the variation in the yield stress with the extrusion ratio became small. This indicates that the deformation-kink-band strengthening effect for the increase in the yield stress largely decreased, especially for the R5 and R10 extruded alloys, as shown in Fig. 12(c). At 400 °C, the yield stress tended to decrease as the extrusion ratio increased, and the yield stress of the extruded alloys showed lower or almost comparable values than that of the as-cast alloy. That is, the texture and deformation-kink-band strengthening effects were both diminished at high temperatures around 400 °C. One of the origins of the decrease in yield stress at and above 300 °C is considered to be related to the activation of nonbasal slip [31]. However, the details on the influence of the kink band boundary against the motion of nonbasal dislocations, i.e. whether the nonbasal slip causes the decrease in the deformation-kink-band strengthening effect or not, has not yet been clarified.

In addition to the influence of nonbasal slip, the deformation microstructures at 400 °C suggest that the decrease in the yield stress at high temperatures is related to the occurrence of localized deformations in the vicinity of the grain boundary (Fig. 8). As a plausible origin which induces this, the occurrence of localized grain-boundary sliding as an accommodation mode of the high-temperature deformation behavior is supposed. It was previously confirmed that in an R10 extruded LPSO-phase alloy, tiny recrystallized LPSO-phase grains were locally formed in the vicinity of grain boundaries during the extrusion process [22]. Thus, it can be expected that the increase in the extrusion ratio enhances the formation of such tiny recrystallized grains and assists the occurrence of localized grain-boundary sliding as an accommodation mode of the high-temperature deformation. The decrease in yield stress with increasing extrusion ratio and the drastic decrease in the differences in the yield stresses in the 0° and 45° loading orientations at 400 °C (Fig. 6(c)) support this assumption. However, further details on this high-temperature deformation mechanism activated in the extruded LPSO-phase alloys have not been clarified yet in the present state. More studies are essentially required to

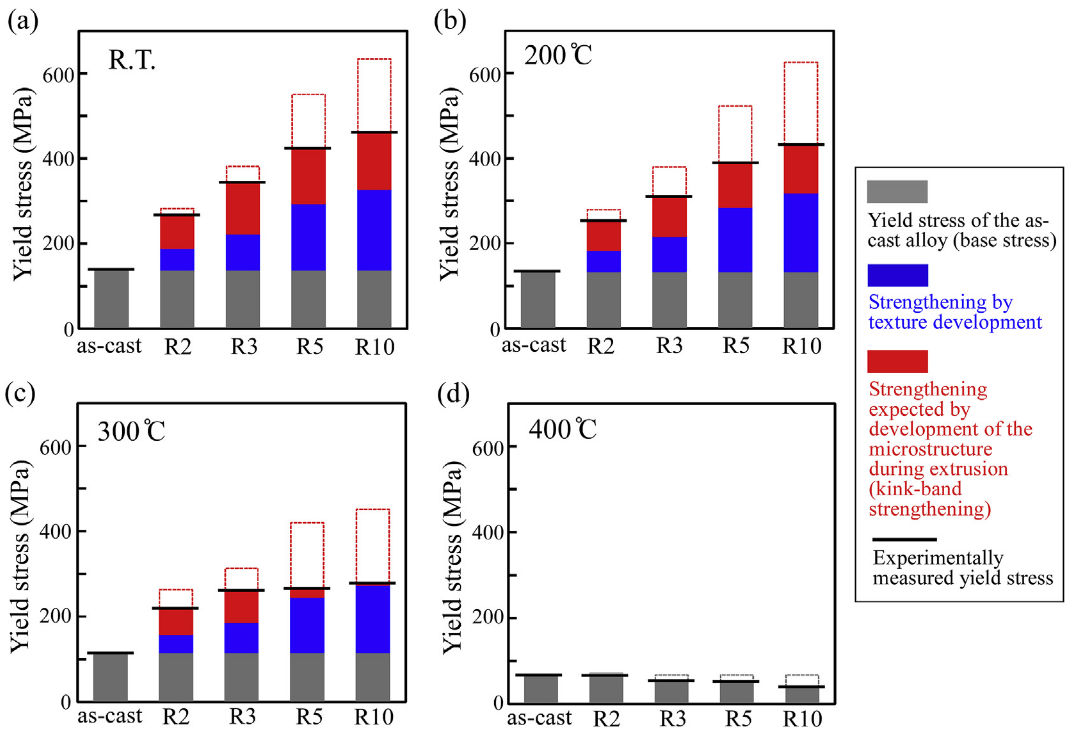

**Fig. 12.** Strengthening factors affecting the yield stresses of the extruded alloys deformed in the 0° orientation at (a) RT, (b) 200 °C, (c) 300 °C, and (d) 400 °C.

elucidate this.

## 5. Conclusion

In this study, the strengthening mechanisms acting in the LPSO-phase alloy induced by extrusion were clarified by compression tests of a $Mg_{88}Zn_4Y_7$ alloy containing a large amount (~86 vol%) of the LPSO phase. The obtained results are summarized as follows:

[1] The yield stress of the extruded LPSO-phase alloy exhibited a strong orientation dependence. The yield stress along the extrusion direction (0° orientation) was much larger than that along the direction inclined at 45° with respect to the extrusion direction (45° orientation) irrespective of the extrusion ratio.

[2] The yield stress increased as the extrusion ratio increased, but the magnitude of the increase in the yield stress was significantly different depending on the loading orientation. That is, the strengthening of the LPSO phase by extrusion shows a strong anisotropy. This was attributed to the variation in the deformation mechanisms depending on the loading orientation and extrusion ratio.

[3] Basal slip governs the deformation behavior of the as-cast and extruded alloys deformed in the 45° orientation. On the other hand, the predominant deformation mechanism varies from basal slip to the formation of deformation kink bands as the extrusion ratio increases in the 0° orientation.

[4] The apparent CRSS for basal slip increases by the introduction of deformation-kink-band boundaries in the LPSO-phase alloys since they effectively act as strong obstacles against the motion of basal slip.

[5] The drastic increase in the yield stress of the LPSO phase alloys in the 0° orientation is brought about by the synergistic effect of the development of the $\{10\bar{1}0\}$ basal fiber texture and the strengthening by the deformation-kink-band boundaries introduced during the extrusion process. In this study, "the kink band strengthening" was first quantitatively elucidated, which contributes to the drastic increase in the yield stress of the LPSO-phase alloys in the wide temperature range below 400 °C.

## Acknowledgement

This work was supported by Japan Society for the Promotion of Science (JSPS) KAKENHI for Scientific Research on Innovative Areas "MFS Materials Science (Grant Numbers: JP18H05478, JP18H05476 and JP18H05475)". This work also partly supported by Cross-Ministerial Strategic Innovation Promotion Program (SIP), Innovative design/manufacturing technologies from New Energy and Industrial Technology Development Organization (NEDO) of Japan.

## References

[1] M.K. Kulekci, Magnesium and its alloys applications in automotive industry, Int. J. Adv. Manuf. Technol. 39 (2008) 851–865.
[2] Y. Kawamura, K. Hayashi, A. Inoue, T. Masumoto, Rapidly solidified powder metallurgy $Mg_{97}Zn_1Y_2$ alloys with excellent tensile yield strength above 600 MPa, Mater. Trans. 42 (2001) 1172–1176.
[3] M. Yamasaki, T. Anan, S. Yoshimoto, Y. Kawamura, Mechanical properties of warm-extruded Mg–Zn–Gd alloy with coherent 14H long periodic stacking ordered structure precipitate, Scripta Mater. 53 (2005) 799–803.
[4] K. Hagihara, A. Kinoshita, Y. Sugino, M. Yamasaki, Y. Kawamura, H.Y. Yasuda, Y. Umakoshi, Effect of long-period stacking ordered phase on mechanical properties of Mg97Zn1Y2 extruded alloy, Acta Mater. 58 (2010) 6282–6293.
[5] X.H. Shao, Z.Q. Yang, X.L. Ma, Strengthening and toughening mechanisms in Mg–Zn–Y alloy with a long period stacking ordered structure, Acta Mater. 58 (2010) 4760–4771.
[6] M. Yamasaki, K. Hashimoto, K. Hagihara, Y. Kawamura, Effect of multimodal microstructure evolution on mechanical properties of Mg–Zn–Y extruded alloy, Acta Mater. 59 (2011) 3646–3658.
[7] E. Oñorbe, G. Garcés, P. Pérez, P. Adeva, Effect of the LPSO volume fraction on the microstructure and mechanical properties of $Mg–Y_{2X}–Zn_X$ alloys, J. Mater. Sci. 47 (2012) 1085–1093.
[8] J. Wang, P. Song, X. Zhou, X. Huang, F. Pan, Influence of the morphology of long-period stacking ordered phase on the mechanical properties of as-extruded Mg–5Zn–5Y–0.6Zr magnesium alloy, Mater. Sci. Eng., A 556 (2012) 68–75.
[9] K. Hagihara, A. Kinoshita, Y. Fukusumi, M. Yamasaki, Y. Kawamura, High-temperature compressive deformation behavior of $Mg_{97}Zn_1Y_2$ extruded alloy containing a long-period stacking ordered (LPSO) phase, Mater. Sci. Eng., A 560 (2013) 71–79.
[10] E. Oñorbe, G. Garcés, F. Dobes, P. Pérez, P. Adeva, High-temperature mechanical behavior of extruded Mg-Y-Zn alloy containing LPSO phases, Metall. Mater. Trans. A 44 (2013) 2869–2883.
[11] L.B. Tong, X.H. Li, H.J. Zhang, Effect of long period stacking ordered phase on the microstructure, texture and mechanical properties of extruded Mg–Y–Zn alloy, Mater. Sci. Eng., A 563 (2013) 177–183.
[12] G. Garces, D.G. Morris, M.A. Muñoz-Morris, P. Perez, D. Tolnai, C. Mendis, A. Stark, H.K. Lim, S. Kim, N. Shell, P. Adeva, Plasticity analysis by synchrotron radiation in a Mg97Y2Zn1 alloy with bimodal grain structure and containing LPSO phase, Acta Mater. 94 (2015) 78–86.
[13] G. Garces, P. Perez, S. Cabeza, H.K. Lin, S. Kim, W. Gan, P. Adeva, Reverse tension/compression asymmetry of a Mg-Y-Zn alloys containing LPSO phases, Mater. Sci. Eng., A 647 (2015) 287–293.
[14] J.K. Kim, S. Sandlöbes, D. Raabe, On the room temperature deformation mechanisms of a Mg-Y-Zn alloy with long-period-stacking-ordered structures, Acta Mater. 82 (2015) 414–423.
[15] H. Liu, J. Bai, K. Yan, J. Yan, A. Ma, J. Jiang, Comparative studies on evolution behaviors of 14H LPSO precipitates in as-cast and as-extruded Mg-Y-Zn alloys during annealing at 773 K, Mater. Des. 93 (2016) 9–18.
[16] E. Abe, A. Ono, T. Itoi, M. Yamasaki, Y. Kawamura, Polytypes of long-period stacking structures synchronized with chemical order in a dilute Mg–Zn–Y alloy, Phil. Mag. Lett. 91 (2011) 690–696.
[17] K. Hagihara, N. Yokotani, Y. Umakoshi, Plastic deformation behavior of $Mg_{12}YZn$ with 18R long-period stacking ordered structure, Intermetallics 18 (2010) 267–276.
[18] K. Hagihara, Y. Sugino, Y. Fukusumi, Y. Umakoshi, T. Nakano, Plastic deformation behavior of $Mg_{12}ZnY$ LPSO-phase with 14H-typed structure, Mater. Trans. 52 (2011) 1096–1103.
[19] K. Hagihara, T. Okamoto, H. Izuno, M. Yamasaki, M. Matsushita, T. Nakano, Y. Kawamura, Plastic deformation behavior of 10H-type synchronized LPSO phase in a Mg-Zn-Y system, Acta Mater. 109 (2016) 90–102.
[20] M. Yamasaki, K. Hagihara, S. Inoue, J.P. Hadorn, K. Kawamura, Crystallographic classification of kink bands in an extruded Mg–Zn–Y alloy using intragranular misorientation axis analysis, Acta Mater. 61 (2013) 2065–2076.
[21] K. Hagihara, M. Yamasaki, M. Honnami, H. Izuno, M. Tane, T. Nakano, Y. Kawamura, Crystallographic nature of deformation bands shown in Zn and Mg-based long period stacking ordered (LPSO) phase, Phil. Mag. 95 (2015) 132–157.
[22] K. Hagihara, A. Kinoshita, Y. Sugino, M. Yamasaki, Y. Kawamura, H.Y. Yasuda, Y. Umakoshi, Plastic deformation behavior of $Mg_{89}Zn_4Y_7$ extruded alloy composed of long-period stacking ordered phase, Intermetallics 18 (2010) 1079–1085.
[23] Z. Leng, J. Zhang, M. Zhang, X. Liu, H. Zhan, R. Wu, Microstructure and high mechanical properties of Mg-9RY-4Zn (RY: Y-rich misch metal) alloy with long period stacking ordered phase, Mater. Sci. Eng., A 540 (2012) 38–45.
[24] Z. Leng, J. Zhang, C. Cui, J. Sun, S. Liu, R. Wu, M. Zhang, Compression properties at different loading directions of as-extruded Mg-9RY-4Zn (RY: Y-rich misch metal) alloy with long period stacking ordered phase, Mater. Des. 51 (2013) 561–566.
[25] G. Garces, M.A. Muñoz-Morris, D.G. Morris, J.A. Jimenez, P. Perez, P. Adeva, The role of extrusion texture on strength and its anisotropy in a Mg-base alloy composed of the Long-Period-Structural-Order phase, Intermetallics 55 (2014) 167–176.
[26] S.M. Zhu, R. Lapovok, J.F. Nie, Y. Estrin, S.N. Mathaudhu, Microstructure and mechanical properties of LPSO phase dominant $Mg_{85.8}Y_{7.1}Zn_{7.1}$ and $Mg_{85.8}Y_{7.1}Ni_{7.1}$ alloys, Mater. Sci. Eng., A 692 (2017) 35–42.
[27] G. Garcés, K. Máthis, J. Medina, K. Horváth, D. Drozdenko, E. Oñorbe, P. Dobroň, P. Pérez, M. Klaus, P. Adeva, Combination of in-situ diffraction experiments and acoustic emission testing to understand the compression behavior of Mg-Y-Zn alloys containing LPSO phase under different loading conditions, Int. J. Plast. 106 (2018) 107–128.
[28] M. Hirano, M. Yamasaki, K. Hagihara, K. Higashida, K. Kawamura, Effect of extrusion parameters on mechanical properties of $Mg_{97}Zn_1Y_2$ alloys at room and elevated temperatures, Mater. Trans. 51 (2010) 1640–1647.
[29] T. Laser, Ch Hartig, M.R. Nürnberg, D. Letzig, R. Bormann, The influence of calcium and cerium mischmetal on the microstructural evolution of Mg–3Al–1Zn during extrusion and resulting mechanical properties, Acta Mater. 56 (2008) 2791–2798.
[30] T. Mayama, M. Noda, R. Chiba, M. Kuroda, Crystal plasticity analysis of texture development in magnesium alloy during extrusion, Int. J. Plast. 27 (2011) 1916–1935.
[31] K. Hagihara, Y. Fukusumi, M. Yamasaki, T. Nakano, Y. Kawamura, Non-basal

slip systems operative in $Mg_{12}ZnY$ long-period stacking ordered (LPSO) phase with 18R and 14H structures, Mater. Trans. 54 (2013) 693–697.

[32] K. Hagihara, T. Okamoto, M. Yamasaki, Y. Kawamura, T. Nakano, Electron backscatter diffraction pattern analysis of the deformation band formed in the Mg-based long-period stacking ordered phase, Scrpta Mater 117 (2016) 32–36.

[33] K. Hagihara, A. Kinoshita, Y. Sugino, M. Yamasaki, Y. Kawamura, H.Y. Yasuda, Y. Umakoshi, Temperature dependence of compressive deformation behavior of $Mg_{89}Zn_4Y_7$ extruded LPSO-phase alloys, Mater. Sci. Forum 654–656 (2010) 607–610.

[34] X.-L. Nan, H.-Y. Wang, L. Zhang, J.-B. Li, Q.-C. Jiang, Calculation of Schmid factors in magnesium: analysis of deformation behaviors, Scripta Mater. 67 (2012) 443–446.

[35] K. Hagihara, M. Honnami, R. Matsumoto, Y. Fukusumi, H. Izuno, M. Yamasaki, T. Okamoto, T. Nakano, Y. Kawamura, In-situ observation on the formation behavior of the deformation kink bands in Zn single crystal and LPSO phase, Mater. Trans. 56 (2015) 943–951.